Available online at www.sciencedirect.com

jmr&t Journal of Materials Research and Technology

journal homepage: www.elsevier.com/locate/jmrt

Original Article

High Si multilayered TiSiN/TiN(Ag) films with superior oxidation resistance

A. AL-Rjoub [a,*], A. Cavaleiro [a,b], S.S. Rajput [c], F. Fernandes [a]

[a] University of Coimbra, CEMMPRE - Centre for Mechanical Engineering Materials and Processes, Department of Mechanical Engineering, Rua Luís Reis Santos, Coimbra, 3030-788, Portugal

[b] IPN - LED&MAT - Instituto Pedro Nunes, Laboratório de Ensaios, Desgaste e Materiais, Rua Pedro Nunes, Coimbra, 3030-199, Portugal

[c] Department of Mechanical Engineering, Indian Institute of Technology Bhilai, Chhattisgarh, 492015, India

ARTICLE INFO

Article history:
Received 11 February 2021
Accepted 14 April 2021
Available online 21 April 2021

Keywords:
TiSiN/TiN(Ag) films
Structure
Thermal stability
Oxidation resistance

ABSTRACT

In this work, the effect of Ag content on the morphology, structure, mechanical properties, thermal stability, and oxidation resistance of multilayered TiSiN/TiN(Ag) films, with Si concentration in the range of 6.3–7.0 at.%, is investigated. The coatings are deposited by DC reactive magnetron sputtering, with increasing Ag content from 0 to 13.9 at.%. All coatings exhibit a face-centered cubic structure (f.c.c NaCl type) and the Ag diffraction peaks progressively increase with increasing Ag content. The hardness and the reduced elastic modulus of the as-deposited films decrease with increasing Ag; these mechanical properties are higher after annealing at 800 °C in protective atmosphere due to the improvement of the crystallinity of the films. The multilayered architecture of the coatings promotes a good barrier against Ag diffusion towards the surface in protective atmosphere. Ag addition does not influence the onset point of oxidation of the films, but it degrades the oxidation resistance due to the Ag diffusion during the oxidation process, which promotes extra paths for ions diffusion.

1. Introduction

The unsuccess of low friction coatings as diamond-like carbon and transition metals compounds for high speed machining under dry conditions, motivated the research on the self-lubricant coatings produced by PVD as a possible solution for overcoming those problems [1]. To accomplish this objective, the solid-lubricant coatings should contribute for solving major problems occur during dry machining, such as, the chemical reactivity between the workpiece and the tool, the low heat conductivity of some hard to machine materials [2–6], the build-up edges [5,7], and the severe shear stresses [7]. Therefore, self-lubricant coatings, by protecting the tools and improving their operation performance under dry machining conditions [8], are potential solutions for several specific applications in the aerospace and automotive industries.

Self-lubricant coatings should combine a set of properties difficult to achieve in a simple material such as, high

* Corresponding author.
E-mail address: abbas.al-rjoub@dem.uc.pt (A. AL-Rjoub).

https://doi.org/10.1016/j.jmrt.2021.04.040

toughness, low friction, good wear-resistance and thermal stability at high temperature [8,9]. Most of the current self-lubricant coatings are deposited as monolayers or multilayered coating systems consist of a high mechanical strength and oxidation resistance of binary or ternary nitrides and/or carbonitrides of transition metals such as: Ti, Cr, W or Ni, alloyed with (i) soft metals (V, Ag, Au, Cu, Ni, etc), (ii) fluorides (CaF_2, BaF_2, and CeF_3) and (iii) metal oxides (V_2O_5, $Ag_2Mo_2O_7$) (see the comprehensive papers in the literature of Voevodin et al. [9], Zhu et al. [10] and Aouadi et al. [11]). The soft element/compound at the surface works as a lubricious material during machining, leading to a decrease in the friction and improving the wear performance [12–15]. Despite of the better wear performance and the decrease of the friction, many of these coatings still do not meet the requirements for high speed machining due to the fast diffusion to the surface of the elements responsible for the lubrication. Therefore, there is a need to find alternatives for better control of the release of the lubricious phase. A multilayered nano-structured arrangement properly designed can work as an efficient barrier to the lubricant diffusion. Moreover, due to the so-called superlattice effect, multilayered coating systems have also been reported to promote better mechanical properties, thermal stability and oxidation resistance in comparison to their corresponding monolayered films [16,17]. In our previous work [18], the influence of Ag alloying on the morphology, structure, mechanical properties, thermal stability and oxidation resistance of multilayered TiSiN/Ti(Ag)N films with low Si and Ag concentrations was studied. The TiSiN layer in the multilayer architecture revealed to be an efficient barrier to the Ag ions diffusion under vacuum conditions. However, under oxygen atmosphere, Ag concentration decreases the oxidation resistance of films due to the Ag diffusion during the oxidation process, which promotes extra paths for ions diffusion and gives rise to a less protective Ti–Si–O layer. Multilayered TiSiN/TiSi(Ag)N films with TiSiN layers with higher Si concentration may provide a better barrier to the ions diffusion either due to the presence of Si_3N_4 phase [19] and/or due to the formation of a Ti–Si–O layer richer in Si, both with better anti-diffusion properties. Such configuration may also allow to increase the Ag concentration in the films, which is required to provide a proper lubrication behavior, without compromising the blocking of the lubricious phase diffusion.

The aim of the present work is to study the effect of Ag addition on the morphology, structure, mechanical properties, thermal stability and oxidation resistance of multilayered TiSiN/TiN(Ag) films with TiSiN and Ti(Ag)N layers with high Si and Ag concentrations, respectively.

2. Experimental

The TiSiN/TiN(Ag) multilayered films with different Ag content were deposited by DC reactive magnetron sputtering. The chamber has two facing up magnetron cathodes with two high-purity (99.9%) Ti targets (10 × 20 cm); (i) one has holes of 1.5 cm in diameter distributed uniformly in the target erosion zone filled with 8 Si pellets, used to deposit the TiSi, TiSiN gradient layer, and TiSiN layers; (ii) In the other one, the holes of 1.0 cm in diameter were filled with Ag pellets, to increase the Ag content in films, and was used to deposit the TiN (in the case of reference coating) and the TiN(Ag) layers. Three coatings were produced (S0, S1 and S2 with 0, 8.8 and 13.9 at.% of Ag, respectively) by filling the holes of the second target with 0, 5, and 10 Ag pellets, respectively, while the remaining holes were filled with Ti pellets. The substrates were: i) FeCrAlY alloy (12 × 8 × 1 mm), to evaluate the thermal stability after annealing, the hardness and the reduced elastic modulus, the structure, as well as the morphology, thickness and chemical composition, ii) Al_2O_3 (10 × 8 × 0.5 mm) for oxidation resistance tests and, iii) polished-⌀ 25 × 0.5 mm AISI 316 to calculate the residual-stresses of the coatings.

The substrates were ultrasonic cleaned in acetone and in alcohol for 15 and 10 min, respectively, and assembled on the substrate holder in the chamber. The chamber was vacuumed down to the base pressure of 2.5 10^{-4} Pa, and the substrates were etched for 50 min in Ar atmosphere (pulsed bias of −500 V and frequency of 250 kHz). During the etching time, both targets were shuttered and cleaned simultaneously (P_{Ar} = 0.27 Pa, 800 W applied to each target). An interlayer and a gradient layer were deposited to improve the adhesion in two steps: i) deposition of a 300 nm adhesive-layer of TiSi (Ar flow of 11 sccm, power density of 6.5 W/cm^2, pulsed bias of −60 V, working pressure of 0.27 Pa and deposition time of 12 min), and ii) deposition of a 230 nm TiSiN gradient layer (Ar flow of 11 sccm, N_2 flow increasing from 1 up to15 sccm, power density of 6.5 W/cm^2, pulsed bias of −60 V, reaching the final working pressure of 0.34 Pa and deposition time of 12 min). Then, the final multilayer-structure was grown immediately (6.5 W/cm^2 on each target, Ar flow of 11 sccm, N_2 flow of 15 sccm, pulsed bias of −60 V, working pressure of 0.34 Pa and deposition time of 1 h 20 min). These deposition parameters were used for all coatings, excepting the number of Ag/Ti pellets in the Ti target. Depending on the individual layers deposition rates, the rotation speed of the substrates holder was lowered from 18 rpm (used for the inter/gradient layers) to 0.9 rpm to produce the TiN(Ag) and TiSiN multilayer structure with a thickness period of ~50 nm (i.e. 25 nm each layer).

Cross-section and surface morphologies as well as the thickness of the films were analyzed by SEM. Chemical composition in random zones of each film's surface was assessed by EDS with an acceleration voltage of 10 keV.

The structure of the films was studied by XRD diffraction using a Cu Kα1 radiation (λ = 1.54060 Å, 45 kV and 40 mA) in 2θ range of 20°–80°, acquired in conventional diffraction mode.

The hardness (H) and the reduced elastic modulus (E) of the films were measured by nano-indentation using a Berkovich diamond pyramid indenter. The indentation depth was <10% of the films thickness, to eliminate the substrate effect, and the tests were carried out with applied loads of 15 mN. A total of 16 measurements for each sample were performed.

The residual stress of the films was calculated from the deflection difference between the coated and uncoated stainless-steel substrates, using the Stoney's equation.

To study the thermal stability, the coatings were annealed in an oven at 800 °C for 2 h in a protective atmosphere (Ar - balance + H_2 - 5 vol%).

The effect of the Ag alloying on the onset oxidation point and the oxidation resistance was studied by thermo-gravimetric

analysis (TGA). The onset point of oxidation of each film was determined by heating the films from room temperature up to 1200 °C with a constant temperature ramp of 20 °C/min, using 50 ml/min of 99.99% purity air. The oxidation weight gain was measured at a regular 2 s intervals in a micro-balance with an accuracy of 0.01 mg. The isothermal oxidation tests were performed in air atmosphere for 2 h at a temperature depending on the determined onset of oxidation.

3. Results and discussion

3.1. Chemical composition

The chemical composition of the multilayered TiSiN–TiN(Ag) films evaluated by EDS is presented in Table 1. All films show a (Ti+4/3Si)/N ratio very close to 1 indicating that N is being bonded following TiN and a-SiN compounds. Nevertheless, the presence of Si in solid solution should not be discarded. Indeed, it is well known from the literature that the structure of the TiSiN films depends on the deposition conditions and on the Si concentration in the films. This system has been reported as consisting of i) a substitutional solid solution of Si in the TiN structure (not predicted by the Ti–Si–N phase diagram) [20–22], ii) a nanocomposite structure composed by fcc crystals of TiN encapsulated by a very thin Si–N amorphous phase [23] and iii) an amorphous structure in the case of high Si concentrations [24]. The solid solution structure has been reported to be formed due to kinetically limited growth conditions, promoted by the low deposition temperature and/or the absence of ion bombardment. Under such conditions, Si adatoms reaching the surface of the growing film, do not possess enough energy to move/diffuse, thus remaining inside the TiN lattice. Above this threshold value, the Si–N phase starts to form. According to J. Houska et al. [24], who conducted classical molecular dynamics simulations to predict thermodynamically preferred structures of Ti (50-x)SixN, the maximum Si content incorporated onto the TiN lattice has been reported to be ~4 at.% of Si. Above this threshold value, the Si–N phase starts to form. Thus as current films were produced at considered low deposition temperature and/or low mobility condition, either presence of Si in solid solution and formation of a-SiN phase is expected [25].

When the Ag pellets are incorporated in the Ti target, the concentration of Ag increases progressively in the films with the consequent decrease in the Ti concentration. Both Si and Ag contents are, comparatively, much higher than the values achieved in our previous work [18]. The higher Si concentration leads to, as it will be shown later, an improvement on the mechanical properties, thermal stability and oxidation resistance of the coatings. Similarly, the increased of the Ag content also can have a positive impact on either the wear performance or the decrease of the friction coefficient of the coatings. The Si concentration of the individual TiSiN layer of the multilayered structure should be close to 10.6 at.%, as measured in the thick monolayer TiSiN film deposited with similar conditions as the multilayered films.

Table 1 – Chemical composition measured by EDS and main properties the films.

Sample	S0	S1	S2	TiSiN Monolayer
N at%	51.2	46.8	44.1	51.8
Ti at%	42.1	37.4	35.7	37.6
Si at%	6.7	7.0	6.3	10.6
Ag at%	0	8.8	13.9	0
(Ti+4/3Si)/N[a]	0.997	0.999	1.0	0.999
Residual stress (GPa)	−4.24	−1.84	−0.8	–
Residual stress (GPa) after annealing	−3.91	−0.15	−0.03	–
Hardness (GPa)	32 ± 4	26 ± 2	18 ± 2	–
Reduced elastic modulus (GPa)	322 ± 22	288 ± 13	252 ± 24	–
Elastic strain to failure - H/E	0.10	0.09	0.07	–

[a] This ratio was calculated considering that Ti and Si are combined as TiN and Si_3N_4 nitrides, respectively.

3.2. Morphology and structure of the coatings

The cross-section and surface morphologies of the multilayered structure, with increasing Ag content in the films, are shown in Fig. 1. The reference TiSiN/TiN multilayered coating of this work shows a denser columnar grain growth, extending from the substrate to the surface, than the TiSiN/TiN multilayered coating deposited in the previous work [18]. When the Ag concentration increased, the columnar structure progressively disappears and the films become denser as shown in Fig. 1b and c. Contrarily, the surface morphology of the films evolves in a different way; the sample S0 shows a tiny and compact cellular-like structure (Fig. 1d), while the Ag incorporation progressively changes to a well-defined cauliflower structure (Fig. 1e and f). As shown in the cross-section images (a-c), the thickness of the films increases with increasing Ag content, as expected due to the higher sputtering rate of silver than Ti. The period thickness of the coatings is around 50 nm (i.e. 25 nm each layer) as calculated from the high-resolution of (a-c) images.

The XRD patterns of the as-deposited multilayered TiSiN/TiN(Ag) coatings and their corresponding TiSiN monolayer acquired in the conventional mode are displayed in Fig. 2a–d). Broad TiN peaks are formed from the cumulative signals of the TiN(Ag) and TiSiN layers, which reveal that the coatings exhibit a face-centered cubic structure phase (fcc NaCl type), as the peaks positions are well fitted with the TiN ICDD card no. 00- 87-633. However, the major contribution for the intensity of the peaks should come from the TiN(Ag) layer since, as shown in Fig. 2d, the TiSiN monolayer with 10.6 at % exhibits low crystallinity with very broad diffraction peaks (quasi-amorphous structure). This agrees well with the model proposed by Patscheider et al. [20], who reported that TiSiN coatings with Si concentrations higher than ~ 10 at.%, are quasi-amorphous. On contrast, the coatings with low Si concentrations in our previous work [18] exhibit crystalline diffraction peaks. Ag-diffraction peaks are also detected in the XRD patterns and their intensities progressively increase with increasing Ag contents. The addition of Ag leads to small shifts of the (111) TiN peak to the right due to the release of the residual stresses, as shown in Table 1, which can be due to the

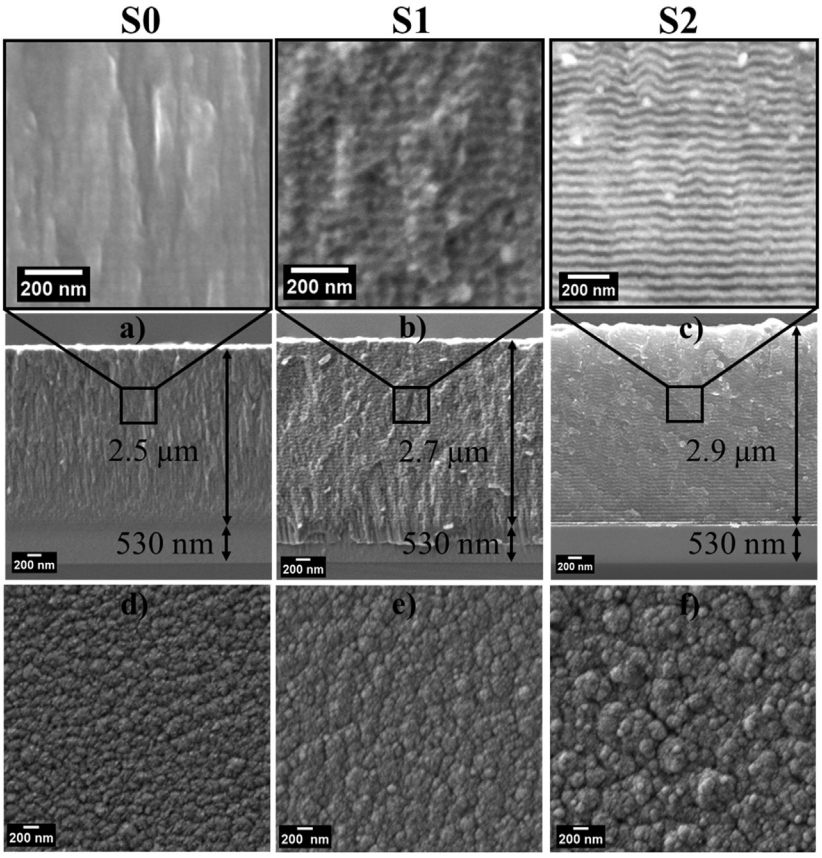

Fig. 1 – Cross-section and surface morphology of S0 to S3 multilayered coatings: a-c) cross section SEM images and their high-resolution images, showing the nano-multilayer structure and d-f) top surface images.

presence of the Ag softer phase in the TiN structure, allowing locally the plastic deformation of the material and the release of the residual stresses. No Si–N crystalline phases are detected in the XRD patterns, suggesting the amorphous character of the Si–N phase, as reported in several works of coating systems contianing Si [20,26–29].

3.3. *Hardness and thermal stability*

The values of hardness (H) and the reduced elastic modulus (E) of the as-deposited and annealed at 800 °C films are presented in Fig. 3. The reference TiSiN/TiN coating (S0) film in the as-

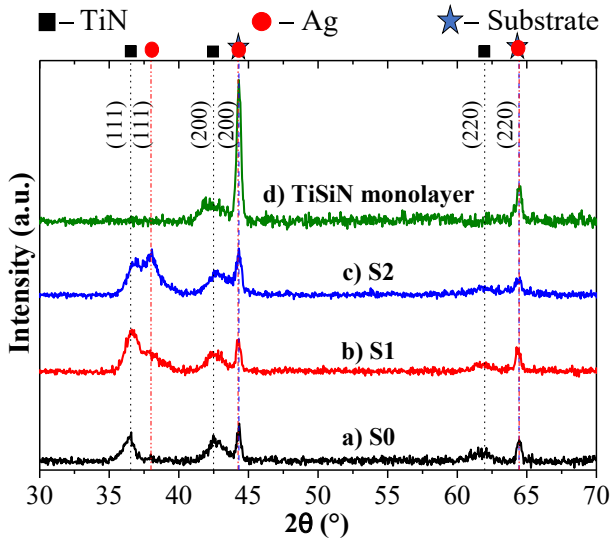

Fig. 2 – XRD diffraction patterns of the coatings obtained in the conventional mode.

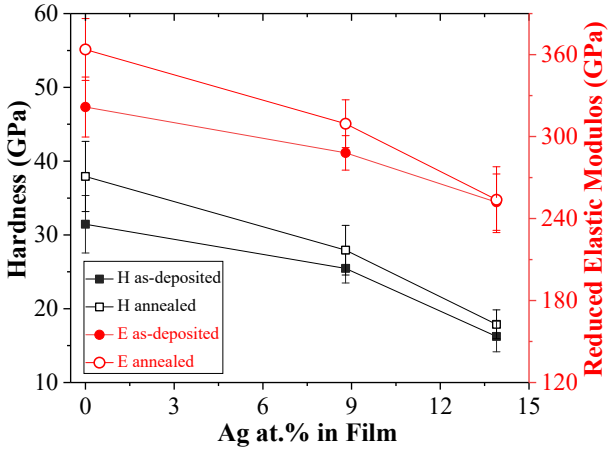

Fig. 3 – a), H and E of as-deposited and annealed films at 800 °C for 2 h.

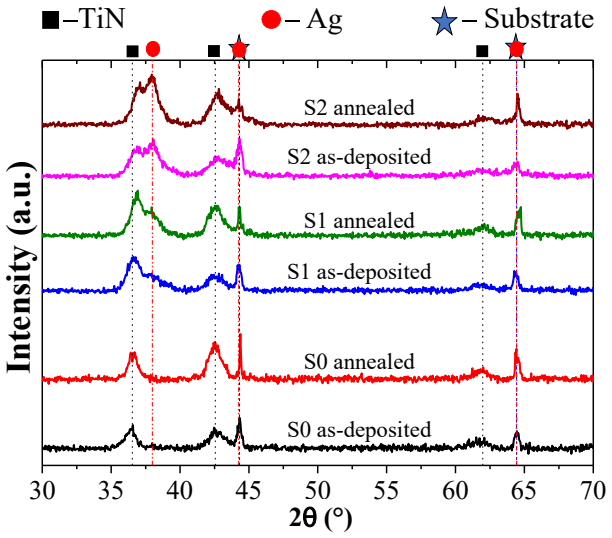

Fig. 4 – XRD diffraction patterns of the coatings in as-deposited and after annealing at 800 °C for 2 h, acquired in conventional mode.

deposited status reveals the highest values of hardness (32 GPa) and reduced elastic modulus (322 GPa). These values are in the range of the values reported by Xu et al. [30], who deposited TiN/TiSiN multilayered system, although with a lower period. Cao et al. [31] deposited harder TiN/TiSiN multilayered coatings (~40 GPa) with a superlattice period of 12 nm. Introducing Ag into the films decreases the H and E values due to the inclusion of a softer phase. Despite of the H and E values are higher in the current work than in our previous one with lower Si and Ag concentration [18], the trend of hardness decrement is the same. After annealing, H and E values of all films increases due to the improvement of the coatings' crystallinity, as reported in the XRD patterns acquired in conventional mode shown in Fig. 4; the patterns do not reveal major changes except the small increase of the peaks' intensities. The small shift to higher diffraction angels, of the TiN peak positions after annealing is due to the release of the residual stresses of the films, as presented in Table 1.

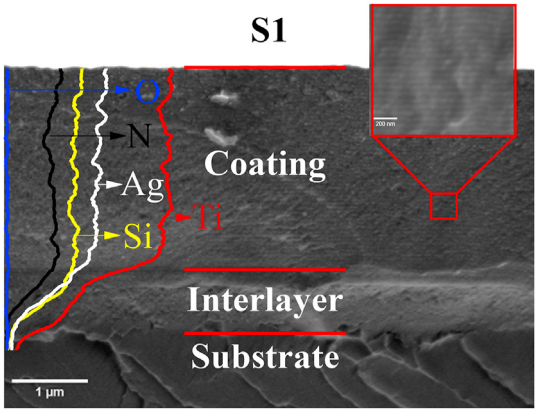

Fig. 5 – Cross-section SEM image of annealed S1 coating and its corresponding EDS line depth profiles.

As shown in Fig. 5, the elemental line profiles through the cross-section and the chemical analysis on the surface of the annealed films (only S1 is shown in the figure) reveal no accumulation of Ag at the surface; the elemental profile remains constant through the films, emphasizing the good control of the Ag diffusion. The concentration of the other chemical elements also remains constant across the thickness of the films. Indeed, the multilayer structure remains visible after annealing, as shown in the magnified insert in Fig. 5.

3.4. *Continuous and isothermal oxidation in air*

Thermo-gravimetric analysis (TGA) tests were carried out for all films to study the effect of the Ag addition on the onset point of oxidation and on the isothermal oxidation resistance. As shown in Fig. 6a, the onset point of oxidation is not affected by the Ag addition (~760 °C). The oxidation kinetics of the reference TiSiN/TiN coating (S0) consists of three steps, i) for temperatures lower than 1000 °C, the oxidation weight gain

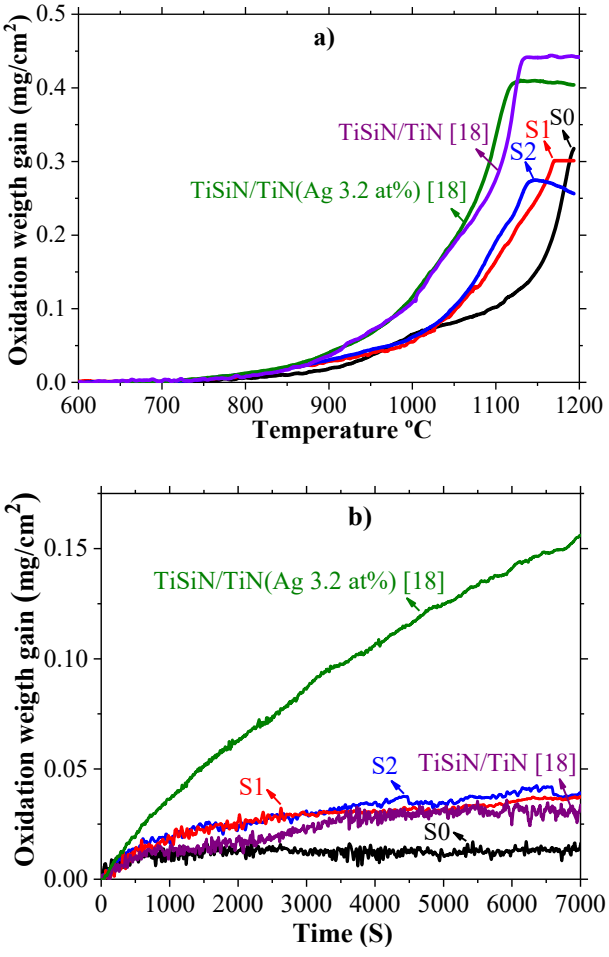

Fig. 6 – a), Thermo-gravimetric oxidation rate of S0, S2 and S3 compared with the TiSiN/TiN and TiSiN/TiN(Ag 3.2 at%) from previous work [18], performed at a constant linear temperature ramp (from RT to 1200 °C at a rate of 20 °C/min) and b) their isothermal TG curves of coatings exposed at 800 °C for 2 h.

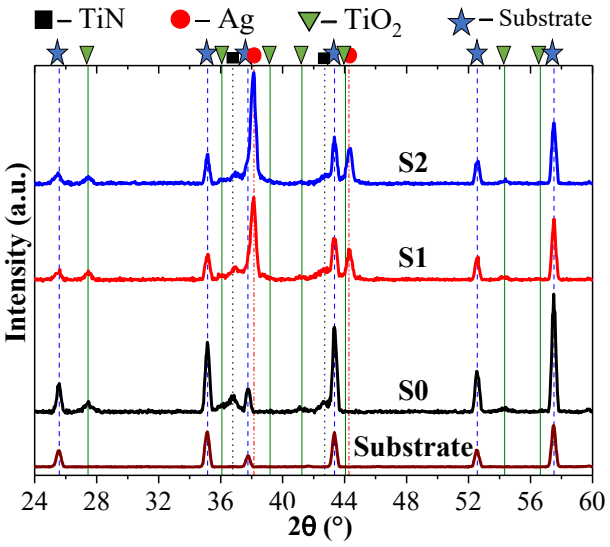

Fig. 7 – XRD diffraction patterns acquired in grazing incidence mode for oxidized S0, S1 and S2 coatings at 800 °C for 2 h. (XRD diffraction of Al_2O_3 substrate is also provided in the figure).

evolves with a progressive growing of the oxidation rate; ii) for temperatures higher than 1000 °C, an inversion in the growing trend of the oxidation rate occurs; the oxidation rate starts to be again very low and, thereafter, grows exponentially with temperature as it is typical with this oxidation test procedure (continuous increasing of the temperature until the complete oxidation of the coating); (iii) for temperature close to 1150 °C, the curve shows strictly higher oxidation rate. The first two steps suggest two different oxidation mechanisms taking place, the first is related with the formation of a less protective oxide layer than in the second.

Although it is not so well marked, these two steps can also be observed in the Ag-containing coatings, with the transition being occurring at approximately 900 °C. Due to the presence of Ag the formed oxides are not so protective and the coatings completely oxidize for lower temperatures.

In comparison with our previous work [18], the oxidation resistance is significantly improved (compare the coatings performance in Fig. 6a) due to the higher Si concentration in the TiSiN layers of the coatings now produced. The presence of higher amount of SiNx phase in the grain boundaries of the TiN grains works as a barrier against the oxygen diffusion and limit the oxidation of TiN. Indeed, the presence of Si gives rise to denser coating's morphology and less defects which, indirectly, make more difficult the reactive species movement with the consequent improvement in the oxidation resistance.

When isothermal tests are concerned, as shown in Fig. 6b, all coatings except the reference one obeyed to a parabolic law of oxidation. The Ag alloyed coatings (S1 and S2) show strictly higher parabolic rate constant than the reference TiSiN/TiN coating (S0). However, these coatings show much better

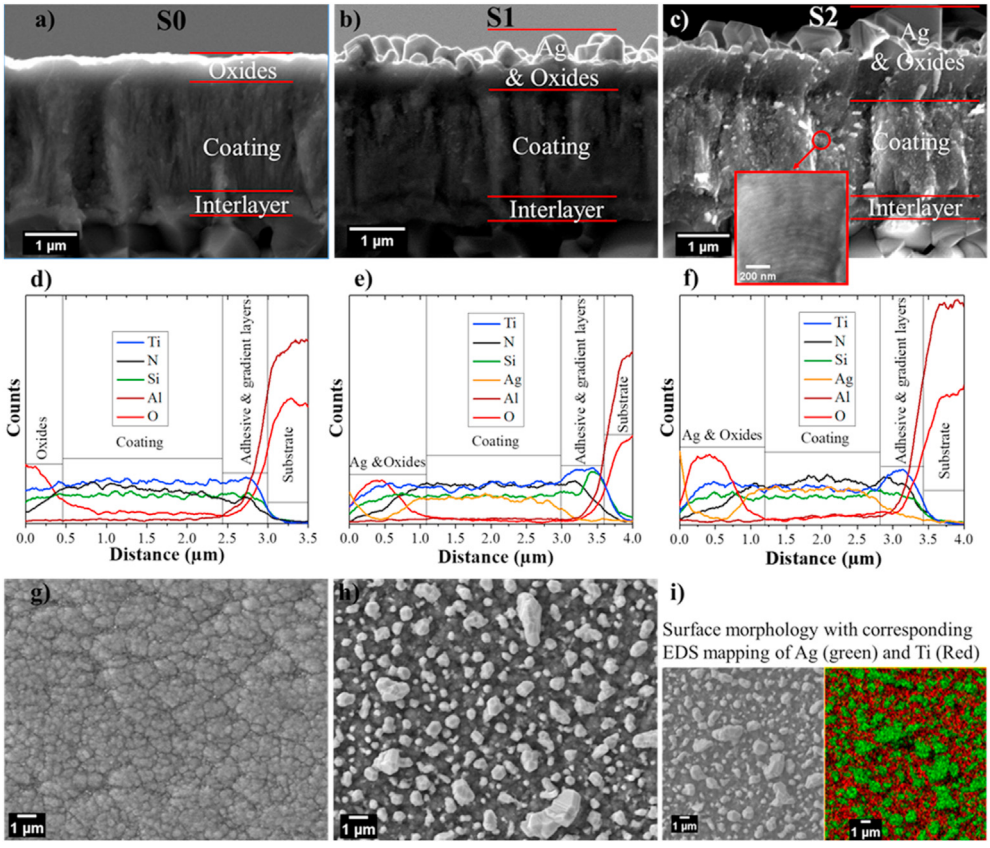

Fig. 8 – Cross-section morphology, corresponding elemental EDS line profiles, and surface morphology of: S0 (a, d and g), S1 (b, e, and h), and S2 (c, f, and i), films.

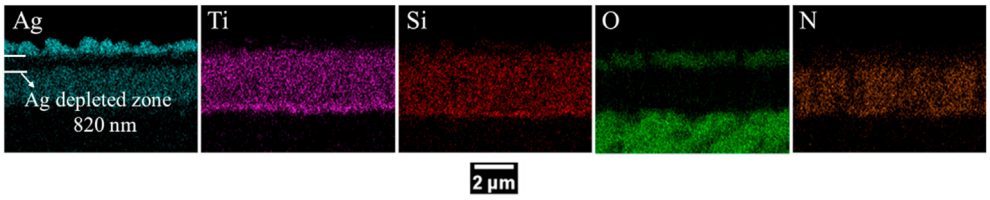

Fig. 9 – Cross section EDS elemental maps distribution of the S2 coating after oxidation at 800 °C for 2 h.

oxidation resistance than those of previous work [18]. This behavior is due to the higher Si concentration as it is reported in several studies about the oxidation of Ti–Si–N coatings (e.g. [32,33]), which showed the role of Si for improving the oxidation resistance of coatings.

XRD diffraction patterns shown in Fig. 7 reveal that all the oxidized films show a mixture of rutile TiO_2 and TiN peaks, suggesting that all films are only partially oxidized. The intensities of Ag peaks of both Ag-containing coatings increase after the oxidation tests. The cross-section analysis and the elemental map distribution shown in Fig. 8 and Fig. 9, respectively, confirm the oxides layers grown on the top surface of the films with thicknesses of ~450 nm, 1.0 μm and 1.3 μm for S0, S1 and S2, respectively. The EDS elemental maps distribution of the S2 film, after oxidation at 800 °C for 2 h shown in Fig. 9, confirms the oxidation on the top of the coating and, most importantly, the presence of Ag accumulated in the top of the oxide layer, corresponding to the under focused big grains shown on the upper part of Fig. 8c. These grains are in the origin of the narrow and high intensity Ag peaks in the diffraction patterns. The oxidation makes the Ag to segregate to the surface leaving behind a ~820 nm depletion zone of Ag. The accumulation of Ag on the surface during the coating's degradation is a promising signal that this solution can work as self-lubrication. Similar behavior was observed in our previous work both TiSi(Ag)N monolayer [34] and TiSiN/Ti(Ag)N multilayered system [18], but with lower Ag and Si contents. An important point to be remarked in relation to previous TiSiN/Ti(Ag)N multilayered system [18] is that, besides the better oxidation resistance of the current, the multilayer structure of the remaining non-oxidized film is maintained after the oxidation test as shown in the magnified image of Fig. 8c.

4. Conclusions

In this work, the effect of Ag alloying of multilayered TiSiN/TiN(Ag) coatings on the morphology, structure, mechanical properties, thermal stability and oxidation resistance is reported. The coatings are produced by DC reactive magnetron sputtering, with increasing Ag contents from 0 up to 13.9 at%. All coatings have N content close to the stoichiometry of the possible formed nitrides, exhibit a face-centered cubic structure (f.c.c NaCl type). The Ag diffraction peaks are progressively more intense with increasing Ag content in the films. On the other hand, the hardness and the reduced elastic modulus of the films decrease due to the incorporation of the softer Ag in the structure. Annealed samples at 800 °C in protective atmosphere result in higher hardness and reduced elastic modulus, in comparison to the as-deposited films, and reveal an excellent thermal stability, e.g. the multilayered structures promote a good barrier for Ag diffusion towards the surface. Ag addition does not influence the onset point of oxidation of the films, but it degrades the oxidation resistance, due to the Ag diffusion during the oxidation process, which promotes extra paths for ions diffusion.

Declaration of competing Interest

The authors declare that they have no known competing financial interests or personal relationships that could have appeared to influence the work reported in this paper.

Acknowledgements

This research is sponsored by FEDER funds through the program COMPETE—Programa Operacional Factores de Competitividade—and by national funds through FCT—Fundação para a Ciência e a Tecnologia—under the projects: CEMMPRE—ref. "UIDB/00285/2020", SMARTLUB—ref. "POCI-01-0145-FEDER-031807", CONTROLLUB—UT Austin Portugal Program ref. "UTAP-EXPL/NTec/0107/2017" and MCTool21 "POCI-01-0247-FEDER-045940". The bilateral collaborative project between Portugal and India (Project number "441.00 INDIA") is also acknowledged.

REFERENCES

[1] Mitterer C, Fateh N, Munnik F. Microstructure-property relations of reactively magnetron sputtered VC_xN_y films. Surf Coating Technol 2011;205:3805–9. https://doi.org/10.1016/j.surfcoat.2011.01.037.

[2] Khanna N, Davim JP. Design-of-experiments application in machining titanium alloys for aerospace structural components. Meas J Int Meas Confed 2015;61:280–90. https://doi.org/10.1016/j.measurement.2014.10.059.

[3] Dandekar CR, Shin YC, Barnes J. Machinability improvement of titanium alloy (Ti-6Al-4V) via LAM and hybrid machining. Int J Mach Tool Manufact 2010;50:174–82. https://doi.org/10.1016/j.ijmachtools.2009.10.013.

[4] Çalişkan H, Küçükköse M. The effect of aCN/TiAlN coating on tool wear, cutting force, surface finish and chip morphology in face milling of Ti6Al4V superalloy. Int J Refract Met Hard Mater 2015;50:304–12. https://doi.org/10.1016/j.ijrmhm.2015.02.012.

[5] Pramanik A. Problems and solutions in machining of titanium alloys. Int J Adv Manuf Technol 2014;70:919–28. https://doi.org/10.1007/s00170-013-5326-x.
[6] Ribeiro Filho SLM, Lauro CH, Bueno AHS, Brandão LC. Influence cutting parameters on the surface quality and corrosion behavior of Ti-6Al-4V alloy in synthetic body environment (SBF) using Response Surface Method. Meas J Int Meas Confed 2016;88:223–37. https://doi.org/10.1016/j.measurement.2016.03.047.
[7] Veiga C, Davim JP, Loureiro AJR. Review on machinability of titanium alloys: the process perspective. Rev Adv Mater Sci 2013;34:148–64.
[8] Renevier NMU, Hamphire J, Fox VC, Witts J, Allen T, Teer DG. Advantages of using self-lubricating, hard , wear-resistant MoS_2 -based coatings. Surf Coating Technol 2001;142–144:67–77. https://doi.org/10.1016/S0257-8972(01)01108-2.
[9] Voevodin AA, Muratore C, Aouadi SM. Hard coatings with high temperature adaptive lubrication and contact thermal management: review. Surf Coating Technol 2014;257:247–65. https://doi.org/10.1016/j.surfcoat.2014.04.046.
[10] Zhu S, Cheng J, Qiao Z, Yang J. High temperature solid-lubricating materials: a review. Tribol Int 2019;133:206–23. https://doi.org/10.1016/j.triboint.2018.12.037.
[11] Aouadi SM, Gao H, Martini A, Scharf TW, Muratore C. Lubricious oxide coatings for extreme temperature applications: a review. Surf Coating Technol 2014;257:266–77. https://doi.org/10.1016/j.surfcoat.2014.05.064.
[12] Fernandes F, Al-Rjoub A, Cavaleiro D, Polcar T, Cavaleiro A. Room and high temperature tribological performance of multilayered tiSiN/TiN and TiSiN/TiN(Ag) coatings deposited by sputtering. Coatings 2020;10:1–13. https://doi.org/10.3390/coatings10121191.
[13] Cavaleiro D, Veeregowda D, Cavaleiro A, Carvalho S, Fernandes F. High temperature tribological behaviour of TiSiN(Ag) films deposited by HiPIMS in DOMS mode. Surf Coating Technol 2020;399:126176. https://doi.org/10.1016/j.surfcoat.2020.126176.
[14] Ju H, Yu D, Yu L, Ding N, Xu J, Zhang X, et al. The influence of Ag contents on the microstructure, mechanical and tribological properties of ZrN-Ag films. Vacuum 2018;148:54–61. https://doi.org/10.1016/j.vacuum.2017.10.029.
[15] Bondarev AV, Kiryukhantsev-Korneev PV, Levashov EA, Shtansky DV. Tribological behavior and self-healing functionality of TiNbCN-Ag coatings in wide temperature range. Appl Surf Sci 2017;396:110–20. https://doi.org/10.1016/j.apsusc.2016.10.188.
[16] Hahn R, Bartosik M, Soler R, Kirchlechner C, Dehm G, Mayrhofer PH. Superlattice effect for enhanced fracture toughness of hard coatings. Scripta Mater 2016;124:67–70. https://doi.org/10.1016/j.scriptamat.2016.06.030.
[17] Rehák P, Holec D, Cerný M. Interface-induced electronic structure toughening of nitride superlattices. Surf Coating Technol 2017;325:410–6. https://doi.org/10.1016/j.surfcoat.2017.06.065.
[18] Al-rjoub A, Cavaleiro A, Fernandes F. Influence of Ag alloying on the morphology, structure, mechanical properties, thermal stability and oxidation resistance of multilayered TiSiN/Ti(Ag)N films. Mater Des 2020;192:108703. https://doi.org/10.1016/j.matdes.2020.108703.
[19] Bilger G, Voss T, Schlenker T, Strohm A. High-temperature diffusion barriers from Si-rich silicon-nitride. Surf Interface Anal 2006;38:1687–91. https://doi.org/10.1002/sia.2396.
[20] Patscheider J, Zehnder T, Diserens M. Structure-performance relations in nanocomposite coatings. Surf Coating Technol 2001;146–147:201–8. https://doi.org/10.1016/S0257-8972(01)01389-5.
[21] Vaz F, Rebouta L, Almeida B, Goudeau P, Pacaud J, Rivière JP, et al. Structural analysis of $Ti_{1-x}Si_xN_y$ nanocomposite films prepared by reactive magnetron sputtering. Surf Coating Technol 1999;120–121:166–72. https://doi.org/10.1016/S0257-8972(99)00450-8.
[22] Fernandes F, Loureiro A, Polcar T, Cavaleiro A. The effect of increasing V content on the structure, mechanical properties and oxidation resistance of Ti – Si–V–N films deposited by DC reactive magnetron sputtering. Appl Surf Sci 2014;289:114–23. https://doi.org/10.1016/j.apsusc.2013.10.117.
[23] Vepfek S, Reiprich S. A concept for the design of novel superhard coatings. Thin Solid Films 1995;268:64–71. https://doi.org/10.1016/0040-6090(95)06695-0.
[24] Houska J, Klemberg-Sapieha JE, Martinu L. Atomistic simulations of the characteristics of TiSiN nanocomposites of various compositions. Surf Coating Technol 2009;203:3348–55. https://doi.org/10.1016/j.surfcoat.2009.04.021.
[25] Fernandes F, Calderon VS, Ferreira PJ, Cavaleiro A, Oliveira JC. Low peak power deposition regime in HiPIMS: deposition of hard and dense nanocomposite Ti-Si-N films by DOMS without the need of energetic bombardment. Surf Coating Technol 2020;397:125996. https://doi.org/10.1016/j.surfcoat.2020.125996.
[26] Athmani M, AL-Rjoub A, Cavaleiro D, Chala A A, Cavaleiro, Fernandes F. Microstructural, mechanical, thermal stability and oxidation behavior of TiSiN/CrVxN multilayer coatings deposited by D.C. reactive magnetron sputtering. Surf Coating Technol 2021;405:126593. https://doi.org/10.1016/j.surfcoat.2020.126593.
[27] AL-Rjoub A, Rebouta L, Cunha NF, Fernandes F, Barradas NP, Alves E. W/AlSiTiNx/SiAlTiOyNx/SiAlOx multilayered solar thermal selective absorber coating. Sol Energy 2020;207:192–8. https://doi.org/10.1016/j.solener.2020.06.094.
[28] Al-Rjoub A, Cavaleiro A, Fernandes F. Structure, morphology, thermal stability and oxidation resistance of multilayered TiSiN/VN films: influence of TiSiN-layer thickness. J Mater Eng Perform 2021:1059–9495. https://doi.org/10.1007/s11665-021-05560-3.
[29] AL-Rjoub A, Costa P, Rebouta L, Cerqueira MF, Alpuim P, Barradas NP, et al. Characterization of magnetron sputtered sub-stoichiometric CrAlSiNx and CrAlSiOyNx coatings. Surf Coating Technol 2017;328:134–41. https://doi.org/10.1016/j.surfcoat.2017.08.038.
[30] Xu YX, Chen L, Liu ZQ, Pei F, Du Y. Improving thermal stability of TiSiN nanocomposite coatings by multilayered epitaxial growth. Surf Coating Technol 2017;321:180–5. https://doi.org/10.1016/j.surfcoat.2017.04.057.
[31] Cao J, Choy K, Sun H, Li H-Q, Teer D, Bao M-D. Syntheses of nano-multilayered TiN/TiSiN and CrN/CrSiN hard coatings. J Coating Technol Res 2011;8(2):283–8. https://doi.org/10.1007/s11998-010-9275-0.
[32] Diserens M, Patscheider J, Le F. Mechanical properties and oxidation resistance of nanocomposite TiN – SiNx physical-vapor-deposited thin films. Surf Coating Technol 1999;121:158–65. https://doi.org/10.1016/S0257-8972(99)00481-8.
[33] Pilloud D, Pierson JF, Lucas MCM De, Cavaleiro A. Study of the structural changes induced by air oxidation in Ti – Si – N hard coatings. Surf Coating Technol 2008;202:2413–7. https://doi.org/10.1016/j.surfcoat.2007.09.017.
[34] Cavaleiro D, Cavaleiro A, Carvalho S, Fernandes F. Oxidation behaviour of TiSiN(Ag) films deposited by high power impulse magnetron sputtering. Thin Solid Films 2019;688. https://doi.org/10.1016/j.tsf.2019.137423.